ACS SENSORS

pubs.acs.org/acssensors

Article

Continuous Small-Molecule Monitoring with a Digital Single-Particle Switch

Junhong Yan,* Laura van Smeden, Maarten Merkx, Peter Zijlstra, and Menno W. J. Prins*

Cite This: *ACS Sens.* 2020, 5, 1168–1176

Read Online

ACCESS | Metrics & More | Article Recommendations | Supporting Information

ABSTRACT: The ability to continuously measure concentrations of small molecules is important for biomedical, environmental, and industrial monitoring. However, because of their low molecular mass, it is difficult to quantify concentrations of such molecules, particularly at low concentrations. Here, we describe a small-molecule sensor that is generalizable, sensitive, specific, reversible, and suited for continuous monitoring over long durations. The sensor consists of particles attached to a sensing surface via a double-stranded DNA tether. The particles transiently bind to the sensing surface via single-molecular affinity interactions, and the transient binding is optically detected as digital binding events via the Brownian motion of the particles. The rate of binding events decreases with increasing analyte concentration because analyte molecules inhibit binding of the tethered particle to the surface. The sensor enables continuous measurements of analyte concentrations because of the reversibility of the intermolecular bonds and digital read-out of particle motion. We show results for the monitoring of short single-stranded DNA sequences and creatinine, a small-molecule biomarker (113 Da) for kidney function, demonstrating a temporal resolution of a few minutes. The precision of the sensor is determined by the statistics of the digital switching events, which means that the precision is tunable by the number of particles and the measurement time.

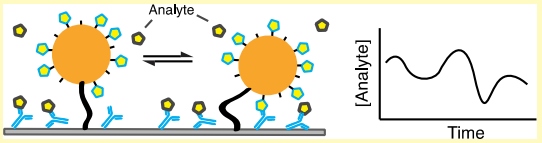

KEYWORDS: *continuous monitoring, small molecule, affinity binder, single-molecule resolution, digital signal, reversible interaction*

Small molecules effectuate a vast variety of biological functions, for example, as substrates and products in metabolic pathways, as cell signaling molecules, and as specific affinity ligands for proteins and membrane receptors.[1] Because of their small size, they can easily permeate into bodily fluids such as interstitial skin fluid, blood plasma, and saliva,[2] making them accessible for diagnostics and monitoring.[3] Continuous monitoring of therapeutic drugs and regulating drug levels via closed-loop control can achieve optimal treatment with a low risk of toxicity for patients.[4] Continuous monitoring of organ function markers[5,6] can serve as early warning for patients with critical or chronic conditions, such as kidney disease, liver disease, or heart disease.

It remains an important challenge to achieve *continuous monitoring* of small molecules, that is, the ability to measure changes in concentrations of small molecules in real time.[7] At present, small-molecule quantification depends on laboratory-based techniques, such as liquid chromatography mass spectrometric assays (LC–MS)[8,9] and affinity-based immunoassays (ELISA).[10] However, LC–MS assays involve extensive sample preparations such as protein precipitation and solid-phase extraction to get reliable results in complex biological matrices. Immunoassays are available on automated laboratory instruments, but the required sample logistics cause turnaround times of hours to days, which strongly limits the applicability for continuous monitoring.

Sensors for continuous monitoring are commercially available for glucose, based on enzymatic electrochemical detection.[11,12] Glucose is present at very high concentrations (millimolar), while many relevant small-molecule analytes are present at much lower concentrations, in the micromolar and nanomolar range.[13,14] Furthermore, enzymes are available only for a limited number of molecules. Therefore, the development is required of more generic sensing principles. Over the past decade, electrochemical aptamer-based sensing has been developed, using aptamers that change conformation upon analyte binding.[15] This method has been demonstrated for therapeutic drugs in live animals, measuring in the low micromolar range.[16] However, conformational probes are not available for all analytes and nanomolar sensitivity has not yet been demonstrated.

In recent work, we introduced a continuous sensing technology called biosensing by particle mobility (BPM), which was developed for the monitoring of macromolecules with at least two sites for affinity binding.[17] Here, a particle is tethered to a sensor surface via a double-stranded DNA molecule, and the particles as well as the sensor surface are functionalized with molecules that bind a specific analyte in a molecular sandwich arrangement. The binding results in confined motion of the particle, which is detected by optical

Received: February 1, 2020
Accepted: March 19, 2020
Published: March 19, 2020

https://dx.doi.org/10.1021/acssensors.0c00220
ACS Sens. 2020, 5, 1168–1176

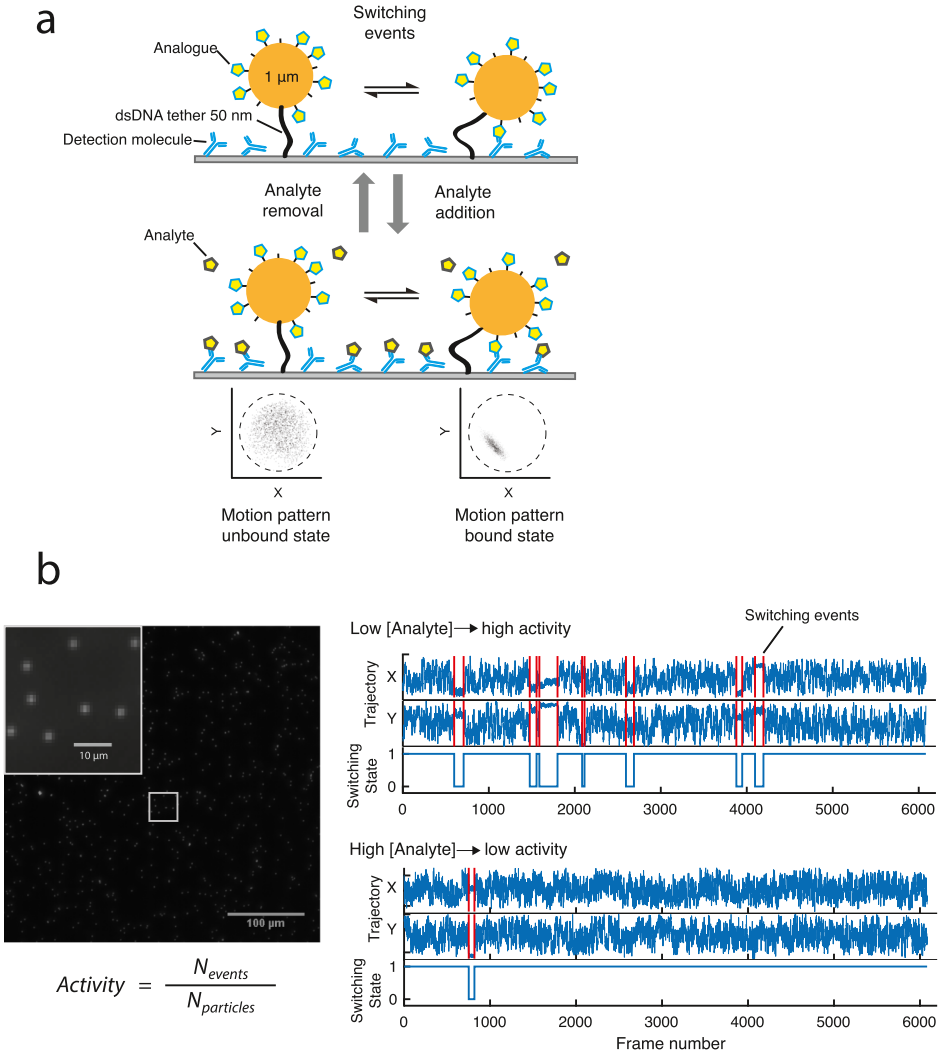

Figure 1. Design of the digital single-particle switch. (a) Schematic drawing of continuous small-molecule monitoring with a digital single-particle switch (the molecules are not to scale). The sensing surface (glass) is coated with detection molecules (reversible affinity binders; here, antibodies against the small-molecule analyte) and is provided with particles that are tethered to the sensing surface via double-stranded DNA. The streptavidin-coated particles are functionalized with the analyte analogue. The sensing functionality is embedded in the digital switching behavior of the particle. The particle dynamically switches between bound and unbound states because of transient binding between the detection molecule and analogues. The state switches are detected by corresponding motion pattern changes, between the unbound state (disk-like motion pattern) and bound state (confined motion pattern). The particle switching dynamics depend on the concentration of the analyte in solution. When the analyte is absent, then detection molecules are available and many particle switching events are recorded. In the case of a high analyte concentration in solution, the detection molecules are blocked by the analyte, resulting in fewer particle switching events. Because of the reversible interactions, the sensor is suited for continuous monitoring of analyte concentration in solution. (b) Hundreds of particles are optically imaged in a field of view of about 400 × 400 μm^2, of which a zoom-in is shown. The reversible interaction between the detection molecules and analogues results in multiple switching events over time, which are tracked by localizing the *X*, *Y* coordinate of the center of the particle. A typical *X*, *Y* trajectory of one particle is shown, for low and high analyte concentration. The red lines indicate switching events identified by an algorithm that analyzes the areal confinement of the particle motion, resulting in a digital time trace of bound (0) and unbound (1) states of the particle. The output parameter of the sensor is activity, which is the number of switching events recorded over a set time period, averaged for the particles within the field of view.

microscopy. Because the molecular sandwich arrangement is reversible, repeated binding and unbinding events are detected as a function of time, which makes the BPM technology suited for continuous monitoring, with a sensitivity and specificity that are determined by the affinity molecules. However, small molecules cannot generally be detected with a molecular sandwich arrangement because the small size of the analytes does not provide enough space for two spatially separated binding sites.

Here, we present a different approach based on a competitive assay, which extends the BPM technology to analytes of arbitrary size. The sensor makes use of analyte analogues immobilized on the particle whose binding to the sensing surface is modulated by the presence of the analyte in solution. We show the continuous detection of short single-stranded DNA (ssDNA) and creatinine, with nanomolar to micromolar sensitivity and a temporal resolution of a few minutes. Comparison of the sensor response to a single-molecule stochastic model shows that the precision of the sensor is limited by the statistics of the digital switching events, providing straightforward means to enhance the precision by increasing the number of probed particles and the measurement time. The presented sensing concept is easily adapted to other analytes, providing a promising technology for

https://dx.doi.org/10.1021/acssensors.0c00220
ACS Sens. 2020, 5, 1168−1176

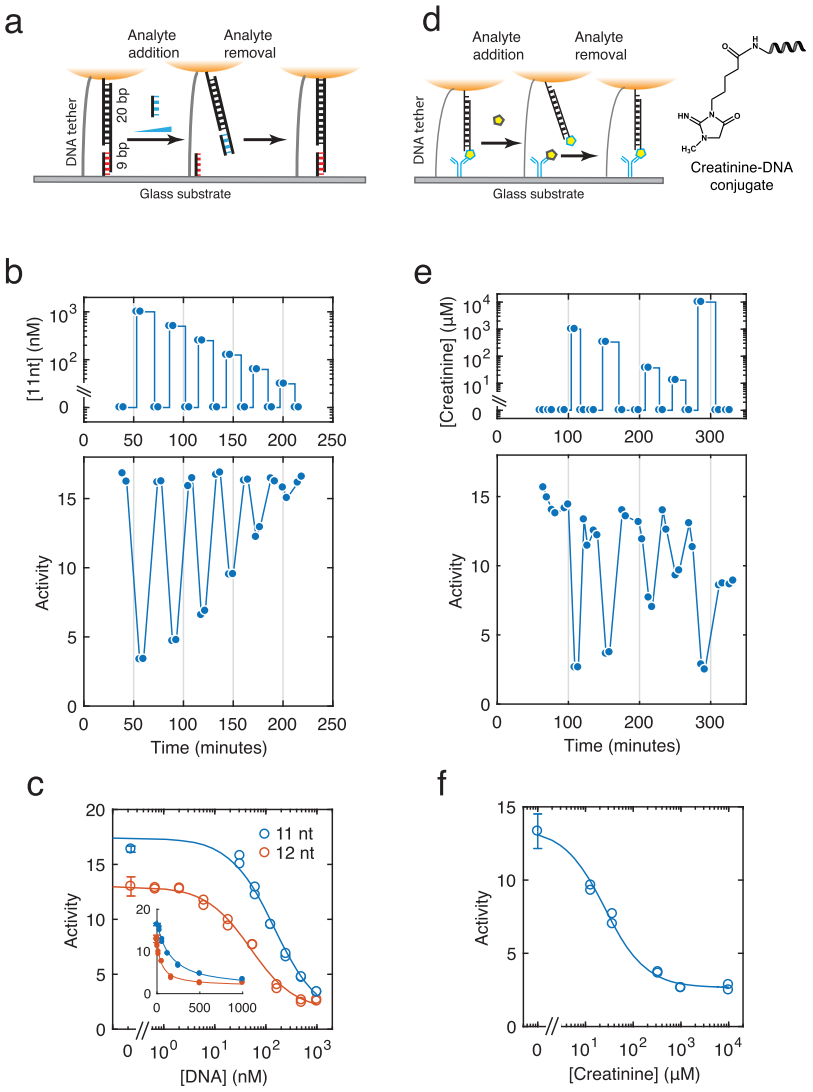

Figure 2. Continuous monitoring of short single-stranded DNA oligonucleotides (a–c) and creatinine (d–f). (a) Schematic drawing of oligonucleotide assay (molecules are not to scale). The sensing surface is functionalized with ssDNA oligonucleotide detection molecules with a 9-nt binding region (in red). Particles are provided with the DNA analogue having 11-nt overhang (in black). The reversible 9 bp hybridization between sensing surface-oligo (red) and DNA analogue results in digital switches of particle mobility in the absence of the analyte. Addition of the 11-nt analyte (in blue) causes blocking of the particle oligo overhang and a reduction of particle switches. The original condition is recovered when the particle is exposed to a solution without the analyte. (b) Particle switching activity as a function of time with an 11-nt analyte in PBS at room temperature. Top: Concentration of DNA analyte as a function of time. Bottom: Measured activity of the sensor. (c) Dose–response curve of 11-nt and 12-nt analytes. The 11-nt data points correspond to panel b. The curves were fitted with a Hill equation with Hill coefficient 1. The IC_{50} for 11-nt and 12-nt are $(1.5 \pm 0.5) \times 10^2$ and $(0.5 \pm 0.2) \times 10^2$ nM, respectively. Zero concentration was measured several times for both 11- and 12-nt over the entire measurement; averages are shown on the graph with error bars indicating the SD (n = 14 for 11-nt and n = 11 for 12-nt). The inset shows the data on linear concentration scale. (d) Schematic drawing of the creatinine assay (molecules are not to scale) and the structure of creatinine–DNA. (e) Particle switching activity as a function of time during sequential aspirations of different concentrations of creatinine in PBS at room temperature. The application of zero concentration after the highest concentration (10 mM) gave incomplete recovery of the signal; this is caused by remaining creatinine (~50 μM) because of incomplete fluid replacement (about 99.5% in our experiment). (f) Dose–response curve for creatinine, established from the data in panel e. The activity of sample in the absence of creatinine was averaged over 18 measurements (except the last point after 10 mM), and error bars indicate the SD.

continuous monitoring in biomedical, industrial, and environmental settings.

RESULTS

The design of the single-particle switch is shown in Figure 1a. A particle (1 μm in diameter) is tethered to a sensing surface via a double-stranded DNA molecule (about 50 nm in length), and the sensing surface is functionalized with detection molecules for recognition of analyte (antibodies in this figure). Analyte analogues, which are molecules similar to the analyte, are immobilized on the particle. The particle moves randomly because of Brownian motion, and molecular bonds can be formed between analyte analogues on the particle and detection molecules on the surface. The reversible binding between analyte analogues and detection molecules causes the particle to switch between bound and unbound states. The bound and unbound states can be distinguished by the motion pattern of the particle, which are disk-like (unbound state) or

https://dx.doi.org/10.1021/acssensors.0c00220
ACS Sens. 2020, 5, 1168–1176

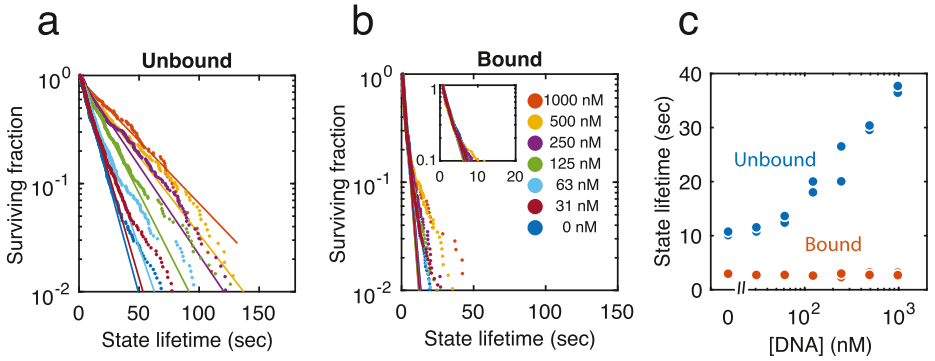

Figure 3. Survival curves of unbound (a) and bound (b) state lifetimes for different oligonucleotide analyte concentrations, in the 11-nt competition assay of Figure 2. Concentrations are indicated in panel b. The curves were fitted with a single-exponential lifetime distribution (solid lines). (c) Dependence of the lifetimes of the unbound (blue) and bound (orange) states on analyte concentration.

more confined (bound state). When analyte is present in solution, they can bind to the detection molecules and thereby reduce the probability per unit time that the particle binds to the surface. Wide-field optical microscopy is used to track hundreds of single particles simultaneously (see Figure 1b), and for each particle, the motion pattern is analyzed by localizing its center of mass in each video frame. Data is analyzed per individual particle as well as for the total ensemble of particles. The average number of switching events per particle recorded over a certain time period, is referred to as the switching activity, or in short, the activity.[17] In the competitive design sketched in Figure 1, the recorded activity is high when there is no analyte in solution and reduces when the analyte concentration increases.

Sensitivity and reversibility of the sensor were first studied for an ssDNA analyte and then applied to continuous monitoring of creatinine (Figure 2). In the DNA assay (Figure 2a), the particles are provided with ssDNA analogues (Figure S1a–c) having 9-nt complementarity to the detection ssDNA on the sensing surface, giving bound state lifetimes in the order of seconds. Figure 2b shows the sensor response in a flow cell experiment, where the sensor was exposed to a sequence of different concentrations of competing ssDNA (analyte) with 11-nt complementarity. The top panel shows the sequence of analyte concentrations with alternating high and zero concentrations. The bottom panel shows the measured activity, which is the average number of switches per particle per measurement window (3 min). When no analyte is present in solution, the so-called blank activity is measured, generated by analogue transiently binding to detection molecules on the glass substrate. The presence of the analyte in solution changes the occupation of the detection molecules according to a Langmuir isotherm (see the Materials and Methods section), so that the activity inversely correlates with the analyte concentration. The experiment shows the reversibility of the competitive assay format, over a total observation time of 4 h. The blank signal (at zero concentration) was measured several times in between analyte concentrations and was used to calibrate the switching activity (see Figure S2). The sensor shows a response time below 5 min, limited in our experiment by the time required to replace the fluid in the flow cell. Figure 2c shows the dose–reponse curves for ssDNA analyte with 11-nt and 12-nt complementarity (time-dependent data of the 12-nt analyte is presented in Figure S3), showing that the 12-nt curve is shifted to lower concentration compared to the 11-nt analyte. The Hill equation fits give IC_{50} values for 11-nt and 12-nt of $(1.5 \pm 0.5) \times 10^2$ and $(0.5 \pm 0.1) \times 10^2$ nM, respectively. This shows that the response of the sensor depends on the affinity of the analyte molecule: a higher affinity gives a higher occupation of detection molecules at the same analyte concentration, in agreement with the Langmuir isotherm. A higher affinity allows the determination of lower analyte concentrations but also results in a lower dissociation rate and therefore a longer response time of the sensor (less than 5 min for 11-nt, ~20 min for 12-nt).

The presented sensor design is adaptable to other analytes by replacing the detection molecules and analogue. After these modifications, the measurements and signal processing proceed identically. As a demonstration, we show in Figure 2d–f the continuous sensing of creatinine, a small molecule (113 Da) with medical importance as a kidney function marker. Creatinine is a byproduct of muscle metabolism and is removed from the blood stream by the kidneys via glomerular filtration. The creatinine concentration in healthy individuals ranges from 40 to 150 μM, related to age, weight, and gender differences, but it can exceed 1000 μM under pathological conditions related to kidney failure.[18] Creatinine is quantified in laboratory instrumentation and point-of-care assays using enzymatic reactions with three or more enzymes that generate either a color change or an electrical current.[19,20] To be able to continuously measure creatinine in the single-particle switch sensor, creatinine-ssDNA conjugates were synthesized in three steps. Creatinine was functionalized with a carboxylic acid via a butyl linker and then conjugated to amine-modified ssDNA via EDC/HOBt/DIPEA chemistry.[21,22] The correct synthesis of creatinine–ssDNA conjugate was verified by mass spectrometry (see Figure S4). Biotinylated antibodies against creatinine were used as the detection molecule on streptavidin-modified glass sensor surfaces. The amount of the detection antibody on the sensor surface was optimized to give a low signal without the analyte analogue and a high signal with the analyte analogue immobilized on the particle (see Figures S1d–f and S5). The flow cell experiment of Figure 2e shows the response of the sensor to a sequence of interchanging high and zero creatinine concentrations in solution. The signal output inversely responds to the concentration input, demonstrating the reversibility of the competitive assay format over a long assay time. Figure 2f shows the dose–response curve with Hill equation fit (IC_{50} of $(2.5 \pm 0.7) \times 10^1$ μM), with a dynamic range of about two decades, matching the medically relevant concentration range of 10–1000 μM. The analytical performance of the assays is summarized in Table S1.

https://dx.doi.org/10.1021/acssensors.0c00220
ACS Sens. 2020, 5, 1168–1176

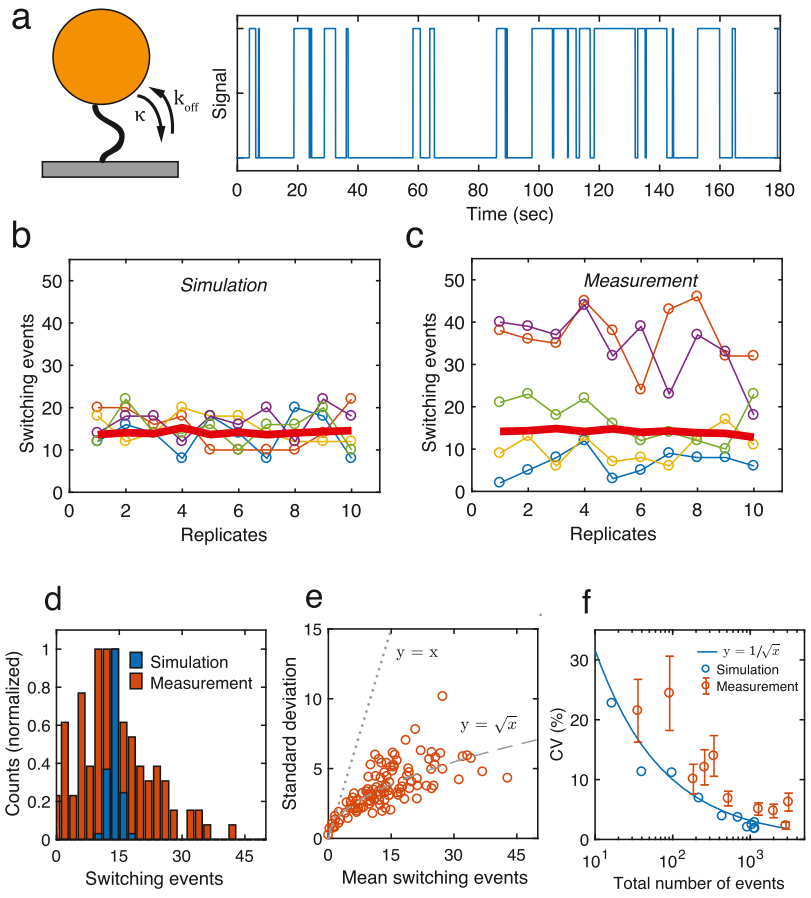

Figure 4. Stochastics and signal variations of the single-particle digital switch sensor. (a) Simulated time trace of one particle with set association (κ) and dissociation (k_{off}) rates that match the measured values. The model assumes Poisson statistics with an exponentially distributed waiting time between events. The low signal corresponds to the immobilized (bound) state. Simulated (b) and measured (c) time traces of five single particles in which events were collected for 3 min. The red lines represent the activity averaged over 100 particles. (d) Distribution of the mean switching events of single particles obtained from the time traces in panels b and c. (e) SD of the switching events of single particles obtained from the measured time traces in panel c. The dotted lines are a guide to the eye and show the scenario when the SD would scale linearly with the mean switching events, or as the square root as expected from Poisson statistics. (f) CV of activity (SD divided by mean) as a function of the total number of detected events across all particles, from the simulated dose–response curve in Figure S7 and measurement data from 10 independent measurements of 3 min over up to 300 particles (Table S2). Error bars are the uncertainty of the CV.

The advantage of a digital switch sensor is that the molecular interactions can be characterized in detail by analyzing the bound and unbound state lifetimes. In the competition-based digital switch sensor, the density of analogues on the particle is chosen such that molecular binding between particle and sensing surface is dominated by reversible single-molecular bonds (the amount of analogues per particle is chosen to be low enough to avoid long-lived multivalent bonds between the particle and substrate). The bonds can be characterized by the bound and unbound state lifetimes extracted from digital switching signals. Figure 3a,b shows the state lifetime survival plots (derived from cumulative distribution functions) for different analyte concentrations, in the 11-nt ssDNA competition assay. In a graph with linear-logarithmic scales, straight lines indicate a single-exponential relationship, characteristic of switching that is caused by a process with a well-defined association rate (for unbound states) or dissociation rate (for bound states). The curves were fitted with a single-exponential equation to determine mean lifetimes that are plotted as a function of analyte concentration in Figure 3c. The bound state lifetime does not depend on the analyte concentration, indicating that in all conditions, the same molecular bond is probed, namely, the 9-bp hybridization between ssDNA on the particle and on the sensor surface. The data show that the lifetimes of about 90% of the bound states follow a single-exponential distribution, independent of the analyte concentration. This indicates that the majority of the bound states result from an interaction between one ligand and one detection molecule. The remaining 10% of bound states has a longer lifetime, which could be caused by multiple molecular bonds or nonspecific bonds. As expected, the unbound state lifetime increases with analyte concentration, caused by the binding of the competing 11-nt ssDNA analyte. A similar dependence of state lifetime on analyte concentration was observed for the creatinine sensor (see Figure S6).

The precision of measurement is a property that needs to be studied for a new biosensing technology. We wanted to investigate what influences the precision, in particular, if variations in the activity signal are limited by fundamental Poisson statistics or whether the variations are determined by other (experimental) factors. To answer that question, we compared simulated and experimental results for 30 min measurements binned in 3 min intervals. In the simulation, we modeled the switching as a stochastic Poisson process with an effective association rate κ and a dissociation rate k_{off}; see Figure 4a. In the simulation, we assume that the binding and

https://dx.doi.org/10.1021/acssensors.0c00220
ACS Sens. 2020, 5, 1168–1176

unbinding of a single particle can be described as a two-state switch in which the lifetime of each state is exponentially distributed with a mean effective switching rate that matches the measured values, $\kappa = 0.1\ s^{-1}$ and $k_{off} = 0.2\ s^{-1}$ in this example. We simulated time traces (Figure 4a) for 100 particles from which the number of switching events and activity were calculated and binned in 3 min intervals to match the experiment.

The open circles show examples of binned switching events from individual particles, whereas the solid red line shows the activity averaged over all 100 particles (Figure 4b,c). The activity level is the same in the simulation and measurement because we use measured rates as input in the model. However, the particle-to-particle variation in switching events is significantly higher in the experiment than in the simulation, which is further highlighted in the histogram of Figure 4d. Particle-to-particle variations in the switching events can be caused, for example, by different numbers and distributions of detection molecules on the particles and the sensor surface, or by surface roughness of the particles. Interestingly, at the level of individual particles, we find that the fluctuations in the number of switching events over 10 measurements scale with the square root of the mean of switching events; see Figure 4e. This indicates that the temporal fluctuations seen for individual particles (as in Figure 4c) are indeed determined by Poisson statistics.

Figure 4f shows the coefficient of variation (CV) of the activity, that is, the standard deviation (SD) divided by the mean, as a function of the number of detected events, from the simulated dose–response curve (shown in Figure S7) and from the measured data (see Table S2). The simulated data scale as the reciprocal square root of the total number of detected switching events, in agreement with Poisson statistics. The curve shows how many events need to be detected to achieve a desired CV. For example, to achieve a CV of 5%, a total of 400 events need to be collected per measurement interval (3–5 min) from all the particles (usually around 400 particles in a typical field of view). The measured CV closely follows the trend of simulated CV with a slight increase. Deviations are possibly caused by event misidentifications in the experiments and also drift of activity over 30 min measurements, which will be further investigated in follow-up research. The main conclusion of these results is that the variations in the replicate measurements can be reduced and a higher precision can be achieved by increasing the number of detected events, so by increasing the duration of the measurement or by observing more particles; the latter can be realized by enlarging the field of view or increasing the density of particles on the surface.

DISCUSSION AND CONCLUSION

For small-molecule BPM sensors to be used in real applications, several aspects need to be further studied. The stability of the sensor needs to be investigated for applications that require unattended operation over long durations. In this paper, DNA and creatinine sensors were studied over a few hours. A gradual reduction of activity was observed in repeated measurements at zero concentration, possibly caused by loss or degradation of detection molecules or analyte analogue, or incomplete fluid exchange after previous supply of the analyte. In future work, we will optimize the fluidics and develop covalent linking chemistries for the respective affinity molecules. Furthermore, the sensor technology will be further developed for use with complex matrices such as blood and fluids extracted from industrial processes, using antifouling strategies to block nonspecific interactions[23,24] and sample filtration with size-exclusion membranes[25] or microdialysis[26,27] to avoid potential interferences from cells and macromolecular aggregates.

In conclusion, we have presented a digital single-particle switch sensor suitable for continuous monitoring, where molecular interactions between particle and sensor surface depend on the concentration of small-molecule analytes in solution. The sensor does not involve enzymatic conversion of the analyte nor specialized conformational probes but relies on reversible affinity interactions that are generalizable to other analytes. Reversible signals were observed in the micromolar range for creatinine and in the nanomolar range for DNA. We envision that the sensor will open up new applications for research in biological sciences,[28–30] patient monitoring,[31] and industrial process monitoring.[32]

MATERIALS AND METHODS

DNA, Protein, and Chemicals. The DNAs used in the study are summarized in Table S3, and they were purchased from IDT. Chemicals used in the study were purchased from Sigma, except if stated otherwise.

Preparation of Creatinine–DNA Conjugates. Creatinine acid was synthesized from creatinine as reported by Arts et al.[21] and characterized by LC–MS. To obtain creatinine–DNA conjugates, 45 μL of 60 mM creatinine acid (Sigma-Aldrich; W387520) was mixed with 4 μL of 60 mM HOBt (Sigma-Aldrich; 54802), 4 μL of 300 mM EDC (Sigma-Aldrich; E6383), and 4 μL of DIPEA (Sigma-Aldrich; 387649) in dimethylsulfoxide (DMSO). The reaction mixture was incubated at room temperature for 15 min. Amine-modified DNA (Short arm) was diluted to 10 μM in MOPS buffer (50 mM MOPS (Sigma-Aldrich; M1254) and 0.5 M NaCl, pH 8.0), of which 72 μL was added to the mixture and left to react for 16 h (room temperature, 850 rpm). A fresh reaction mixture of creatinine acid, HOBt, EDC, and DIPEA was prepared as before, incubated for 15 min, added to the amine–DNA mixture and left to react for 6 h. The reaction was quenched by adding 25 μL of 500 mM NH_4OAc (Sigma-Aldrich; A1542). The reaction mixture containing creatinine–DNA was dissolved in 0.15 mM NaCl in 98% ethanol, stored at −20 °C for 16 h, followed by spinning down at 17,000*g* for 15 min at 4 °C. The pellet was washed a second time (0.15 mM NaCl in 98% ethanol), incubated at −20 °C for 75 min, centrifuged, and washed with 70% ethanol. After incubation at −20 °C for 75 min, it was centrifuged, and the creatinine–DNA was obtained after lyophilization. The creatinine–DNA was dissolved to 25 μM and further purified via spin filtration (3 K 500 μL Amicon spin filter). Purified creatinine–DNA conjugates were analyzed using mass spectrometry by flow injection analysis on a LCQ Fleet (Thermo Finnigan) ion-trap mass spectrometer in the negative mode with 1:1 isopropanol/water + 1% triethylamine (pH 10); 5 μL of 10 μM creatinine–DNA was directly injected, and deconvoluted m/z spectra were obtained with MagTran 1.03 software. Finally, the creatinine–DNA was dissolved to 25 μM and mixed with equal volume of 25 μM long arm oligonucleotide in phosphate-buffered saline (PBS) and ready for analogue binding.

Biotinylation of Antibody. The antibody (2 mg/mL) was first buffer-exchanged to PBS with Zeba Spin Desalting Columns, 7k MWCO (89882, Thermo Fisher Scientific) according to manufacturer's instruction. EZ-Link NHS-PEG_4-biotin was dissolved in DMSO at a final concentration of 4 mM. Then, 10-fold molar excess of NHS-PEG_4-biotin was added to the antibodies and incubated at room temperature for 1 h. Then, excess NHS-PEG_4-biotin was removed by Zeba Spin Desalting Columns, 7k MWCO (89882, Thermo Fisher Scientific), and the biotinylated antibodies are stored

https://dx.doi.org/10.1021/acssensors.0c00220
ACS Sens. 2020, 5, 1168–1176

in PBS with 0.1% bovine serum albumin (BSA) at a concentration of 1 μM.

Functionalization of Particles. To prepare the tether, the main tether was mixed with the end tether at final concentrations of 1 and 2 μM in PBS. The mixture was heated to 95 °C for 3 min and gradually lowered to 25 °C for 20 min. The tether was diluted to 2 nM and ready for particle functionalization. For particle functionalization, 5 μL of the streptavidin-coated magnetic particles (10 mg/mL, Dynabeads MyOne Streptavidin C1, Thermo Scientific) were incubated with 5 μL partial dsDNA tether (prepared before) at a concentration of 2 nM in PBS buffer solution for 30 min on rotating fins (VWR, The Netherlands). The particle mixture was washed three times with 500 μL PBST (PBS with 0.05% Tween 20) and reconstituted in 10 μL PBS. Next, 5 μL PBS with 10 μM of particle binder 20nt was added to the particle mixture and incubated on rotating fins for 30 min. Then, 10 μL mPEG-biotin (PG1-BN-1k, Nanocs) of 100 μM in PBS was incubated with the particle mixture for 5 min. After that, the particle mixture was washed three times with 500 μL PBST (PBS with 0.05% Tween 20), reconstituted in 500 μL assay buffer (PBS with 1% BSA filtered with a 0.22 μm filter and degassed in a vacuum desiccator) and kept on the rotating fin for 30 min. Finally, the particle mixture was sonicated with 10 pulses at 70% with 0.5 duty cycle (Hielscher, Ultrasound Technology).

Functionalization of Streptavidin-Coated Glass. The streptavidin-coated glass NEXTERION Slide HS (1087816, SCHOTT Technical Glass Solutions GmbH) was first washed with PBS for 1 min with the measurement chamber attached to the glass. The glass was then incubated with biotinylated Tether capture oligonucleotide (2.5 nM in PBS) for 30 min. For the DNA system, double-stranded detection oligonucleotides were prepared by mixing 40 μL Detection oligo docking (100 μM) and 10 μL Docking strand 20-nt (100 μM) for 30 min in room temperature and then diluted to 500 nM in PBS according to the concentration to Docking strand 20-nt. Double-stranded detection oligonucleotides were added to the glass and incubated for 30 min. Then, assay buffer was aspirated and incubated for 30 min. For the creatinine assay, the biotinylated anti-creatinine antibody (5 nM in PBS) was added to the glass and incubated for 30 min. Afterward, two steps of blocking were carried out in assay buffer with first neutravidin (2 μM) for 30 min and then biotin polyT (10 μM) for 30 min.

Finally, the functionalized particles were added to the glass to form tethered particles. The incubation time was 1 h for the DNA system and 30 min for the creatinine system. Untethered particles were then washed away by PBS with the glass flipped upside down. The withdrawal speed for the syringe pump was 300 μL/min during glass functionalization and 100 μL/min after particle incubation. The internal volume of the flow cell is 65 μL, and the total surface area of the substrate inside the flow cell is 1.6 mm^2.

Analogue Binding to Particle and Measurement of Analyte. The tethered particles were provided with analogues by aspirating DNA analogues (250 pM) for the DNA system and creatinine−DNA conjugates (50 and 100 pM) for the creatinine system and incubated for 30 min to 1 h. Excess DNA analogues or creatinine−DNA were washed away by aspirating PBS into the flow cell. Concentration series of analyte (DNA Competitor11nt, Competitor12nt, or creatinine) were prepared in PBS and aspirated sequentially into the flow cell. The withdrawal speed for the syringe pump was 100 μL/min during analogue binding and analyte addition. The flow was stopped during measurement.

Image Recording and Data Analysis. Videos were recorded before, during, and after analogue binding, and after each concentration change, on a Nikon Ti-E inverted microscope (Nikon Instruments Europe BV, The Netherlands), at a total magnification of 20× using an iXon Ultra 897 EMCCD camera (Andor, Belfast, UK). The particle motion in a field of view of 405 × 405 μm^2 was recorded for 3, 5, or 30 min at a frame rate of 33.7 Hz with 5 ms exposure time under dark-field illumination conditions with Nikon NIS-Elements software.

Detection and analysis of particle motion and the detection of switching events were described in the previous publication.[17] Motion patterns of the particles were selected by criteria (major amplitude less than 150 nm, symmetry larger than 0.33, radial confinement less than 0.2) to exclude particles with too large, asymmetrical, or ring-shaped motions. Switching events of particles passing selection were included for activity analysis. In the continuous monitoring experiment, blank signal levels were measured repeatedly in between analyte injections. A linear fit of blank activity signal versus time was used to calculate the loss of activity and correct for the drift (see Figure S2a).

Dose−response curves were fitted with a Hill equation, with Hill coefficient $n = 1$

$$A = A_{\min} + \frac{A_{\max} - A_{\min}}{1 + \frac{C}{IC_{50}}}$$

Here, A is the activity and C is the concentration of the analyte. $A_{\max}$ is the maximum activity when there is no analyte, and $A_{\min}$ is the minimum activity at infinite concentration of the analyte. IC_{50} is the analyte concentration causing a 50% inhibition of the activity amplitude $A_{\max} - A_{\min}$.

The CV is calculated as the SD divided by the mean (mean). The uncertainty of CV (σ_{CV}) is calculated with propagation of uncertainties, from the uncertainty of the mean (σ_{mean}, standard error of the mean) and the uncertainty of SD (σ_{SD}), which is the error of fitting the measurement replicates into a normal distribution.

$$\sigma_{CV} \approx CV \cdot \sqrt{\left(\frac{\sigma_{mean}}{mean}\right)^2 + \left(\frac{\sigma_{SD}}{SD}\right)^2}$$

The state lifetime, that is, the number of frames or seconds between two detected events, was analyzed by first separating the bound and unbound states using area ratio neighboring comparison (see Figure S8). The area ratio was defined as the convex hull area of each state divided by the convex hull area of the total measurement frames. If the area ratio of one state is less than the previous and following state, then this state is recognized as a bound state. If the area ratio of one state is more than the previous and following state, then this state is recognized as an unbound state. For the first and the last state in the measurement, the comparison was only carried out with their following or previous state. If these conditions do not apply, then the state is attributed as unidentified. Particles with less than two switching events, and the first and the last of the switching states, were excluded from the analysis. Bound and unbound state lifetimes were collected and plotted in a survival plot and fitted with a single-exponential equation: $a \cdot \exp(-k \cdot t)$. Lifetimes were calculated as $1/k$ from the single exponential fit.

Stochastic Simulations. The response of a competitive sensor was simulated using a stochastic model. The model assumes that association and dissociation are random (thermally activated) processes that follow Poisson statistics. We first generate a time trace in which the lifetimes of the bound and unbound states were exponentially distributed. The random numbers generated from the exponential distribution have a mean effective association and dissociation rate (κ^0_{on} and k^0_{off}, both units [s^{-1}]) that describe the interactions of the particle with the underlying sensing surface. The superscript indicates that these are rates in the absence of the analyte. These rates depend in a complex way on the particle size and shape, distribution of binding sites on the particle and the sensing surface, and the proximity of the particle to the sensing surface. We used mean rate constants that match the measured values ($\kappa^0_{on} = 0.1\ s^{-1}$ and $k^0_{off} = 0.2\ s^{-1}$). The activity (defined throughout as the number of events per 3 min) is determined for individual particles from their respective time traces (see Figure 4a for an example).

The kinetics of the sensor in the presence of the analyte were simulated by assuming that a large number of binding sites on the particle are available for analyte binding. This assumption is based on an estimated number of 30,000 binding sites per particle, of which 1% faces the sensing surface. This results in 300 binding sites being available to bind to the underlying detection molecules (Figure S9). In this limit of a large number of binding sites, the presence of the analyte reduces κ^0_{on} according to the fraction of sites that is occupied

https://dx.doi.org/10.1021/acssensors.0c00220
ACS Sens. 2020, 5, 1168−1176

by the analyte. This fraction is determined using the Langmuir isotherm, in which the fraction of bound sites is given by $f_b = \frac{C}{K_D + C}$, with C being the analyte concentration and K_D being the analyte affinity (set to 100 nM to correspond to the measured affinity). This results in a particle association rate that scales with the bound fraction of sites as $\kappa_{on} = \kappa_{on}^0(1 - f_b) = \kappa_{on}^0 \frac{K_D}{K_D + C}$. The particle dynamics in the presence of the analyte then proceeds as outlined above, with κ_{on}^0 replaced by κ_{on}.

■ ASSOCIATED CONTENT

Supporting Information

The Supporting Information is available free of charge at https://pubs.acs.org/doi/10.1021/acssensors.0c00220.

Supplementary information of sensor preparations for the BPM competition assays, correction of activity drift over time, particle switching activity as a function of time with the 12-nt oligonucleotide, synthesis of the creatinine conjugate, titration of the creatinine antibody on the glass substrate for the creatinine competition assay, survival curves for different creatinine concentrations, simulated dose-response curve, switching state recognition from detected events, estimation of number of accessible molecules on the particle, summary of analytical performance of the competition assays, measurement data of 11-nt DNA competition assay with 10 replicates and calculated CV, and oligonucleotide sequences and modification (PDF)

■ AUTHOR INFORMATION

Corresponding Authors

Junhong Yan − *Department of Biomedical Engineering and Institute for Complex Molecular Systems (ICMS), Eindhoven University of Technology, Eindhoven 5612 AZ, The Netherlands;* orcid.org/0000-0002-2332-2315; Email: junhongyan826@gmail.com

Menno W. J. Prins − *Department of Biomedical Engineering, Department of Applied Physics, and Institute for Complex Molecular Systems (ICMS), Eindhoven University of Technology, Eindhoven 5612 AZ, The Netherlands;* orcid.org/0000-0002-9788-7298; Email: m.w.j.prins@tue.nl

Authors

Laura van Smeden − *Department of Biomedical Engineering and Institute for Complex Molecular Systems (ICMS), Eindhoven University of Technology, Eindhoven 5612 AZ, The Netherlands*

Maarten Merkx − *Department of Biomedical Engineering and Institute for Complex Molecular Systems (ICMS), Eindhoven University of Technology, Eindhoven 5612 AZ, The Netherlands;* orcid.org/0000-0001-9484-3882

Peter Zijlstra − *Department of Applied Physics and Institute for Complex Molecular Systems (ICMS), Eindhoven University of Technology, Eindhoven 5612 AZ, The Netherlands;* orcid.org/0000-0001-9804-2265

Complete contact information is available at: https://pubs.acs.org/10.1021/acssensors.0c00220

Notes

The authors declare the following competing financial interest(s): M.M., P.Z., and M.W.J.P. are listed as inventors on patent application WO/2016/096901 (Biosensor based on a tethered particle). J.Y. and M.W.J.P. are cofounders of Helia Biomonitoring BV that has a license to this patent. All authors declare no further competing interests.

■ ACKNOWLEDGMENTS

We thank Human Gesellschaft für Biochemica und Diagnostica mbH for kindly providing the anti-creatinine antibody. We acknowledge support from NWA Startimpuls Meten en Detecteren, Metropoolregio Eindhoven project "Biosensor voor continu monitoren", and the Safe-N-Medtech H2020 project under grant agreement no. 814607. P.Z. acknowledges financial support from The Netherlands Organisation for Scientific Research (NWO VIDI).

■ REFERENCES

(1) Lodish, H.; Berk, A.; Zipursky, S. L.; Matsudaira, P.; Baltimore, D.; Darnell, J. *The Molecules of Life. Molecular Cell Biology*, 4th ed.; W. H. Freeman: New York, 2000.

(2) Heikenfeld, J.; Jajack, A.; Feldman, B.; Granger, S. W.; Gaitonde, S.; Begtrup, G.; Katchman, B. A. Accessing Analytes in Biofluids for Peripheral Biochemical Monitoring. *Nat. Biotechnol.* **2019**, *37*, 407−419.

(3) Kim, J.; Campbell, A. S.; de Ávila, B. E.-F.; Wang, J. Wearable Biosensors for Healthcare Monitoring. *Nat. Biotechnol.* **2019**, *37*, 389−406.

(4) Rawson, T. M.; O'Hare, D.; Herrero, P.; Sharma, S.; Moore, L. S. P.; de Barra, E.; Roberts, J. A.; Gordon, A. C.; Hope, W.; Georgiou, P.; et al. Delivering Precision Antimicrobial Therapy through Closed-Loop Control Systems. *J. Antimicrob. Chemother.* **2018**, *73*, 835−843.

(5) Poscia, A.; Messeri, D.; Moscone, D.; Ricci, F.; Valgimigli, F. A novel continuous subcutaneous lactate monitoring system. *Biosens. Bioelectron.* **2005**, *20*, 2244−2250.

(6) Schierenbeck, F.; Nijsten, M. W. N.; Franco-Cereceda, A.; Liska, J. Introducing Intravascular Microdialysis for Continuous Lactate Monitoring in Patients Undergoing Cardiac Surgery: A Prospective Observational Study. *Crit. Care* **2014**, *18*, R56.

(7) Ruckh, T. T.; Clark, H. A. Implantable Nanosensors: Toward Continuous Physiologic Monitoring. *Anal. Chem.* **2014**, *86*, 1314−1323.

(8) Tiller, P. R.; Romanyshyn, L. A.; Neue, U. D. Fast LC/MS in the Analysis of Small Molecules. *Anal. Bioanal. Chem.* **2003**, *377*, 788−802.

(9) Sullivan, M. P. *LC/MS Methods for Small Molecule Biomarkers; Translating Molecular Biomarkers into Clinical Assays*; Springer, 2016; pp 99−113.

(10) Wang, X.; Cohen, L.; Wang, J.; Walt, D. R. Competitive Immunoassays for the Detection of Small Molecules Using Single Molecule Arrays. *J. Am. Chem. Soc.* **2018**, *140*, 18132−18139.

(11) Allen, N.; Gupta, A. Current Diabetes Technology: Striving for the Artificial Pancreas. *Diagnostics* **2019**, *9*, 31.

(12) De Bock, M.; McAuley, S. A.; Sundararajan, V.; Lee, M. H.; Paldus, B.; Ambler, G. R.; Bach, L. A.; Burt, M. G.; Cameron, F. J.; Clarke, P. M.; et al. Effect of 6 Months of Hybrid Closed-Loop Insulin Delivery in Adults with Type 1 Diabetes: A Randomised Controlled Trial Protocol. *BMJ Open* **2018**, *8*, No. e020275.

(13) Li, H.; Sørensen, J. V.; Gothelf, K. V. Quantitative Detection of Digoxin in Plasma Using Small-Molecule Immunoassay in a Recyclable Gravity-Driven Microfluidic Chip. *Adv. Sci.* **2019**, *6*, 1802051.

(14) Yu, Q.; Xue, L.; Hiblot, J.; Griss, R.; Fabritz, S.; Roux, C.; Binz, P.-A.; Haas, D.; Okun, J. G.; Johnsson, K. Semisynthetic Sensor Proteins Enable Metabolic Assays at the Point of Care. *Science* **2018**, *361*, 1122−1126.

(15) Baker, B. R.; Lai, R. Y.; Wood, M. S.; Doctor, E. H.; Heeger, A. J.; Plaxco, K. W. An Electronic, Aptamer-Based Small-Molecule Sensor for the Rapid, Label-Free Detection of Cocaine in Adulterated

Samples and Biological Fluids. *J. Am. Chem. Soc.* **2006**, *128*, 3138−3139.
(16) Arroyo-Currás, N.; Somerson, J.; Vieira, P. A.; Ploense, K. L.; Kippin, T. E.; Plaxco, K. W. Real-Time Measurement of Small Molecules Directly in Awake, Ambulatory Animals. *Proc. Natl. Acad. Sci. U.S.A.* **2017**, *114*, 645−650 h.
(17) Visser, E. W. A.; Yan, J.; Van IJzendoorn, L. J.; Prins, M. W. J. Continuous Biomarker Monitoring by Particle Mobility Sensing with Single Molecule Resolution. *Nat. Commun.* **2018**, *9*, 2541.
(18) Waikar, S. S.; Bonventre, J. V. Creatinine Kinetics and the Definition of Acute Kidney Injury. *J. Am. Soc. Nephrol.* **2009**, *20*, 672−679.
(19) Killard, A. J.; Smyth, M. R. Creatinine Biosensors: Principles and Designs. *Trends Biotechnol.* **2000**, *18*, 433−437.
(20) Tsuchida, T.; Yoda, K. Multi-Enzyme Membrane Electrodes for Determination of Creatinine and Creatine in Serum. *Clin. Chem.* **1983**, *29*, 51−55.
(21) Arts, R.; Ludwig, S. K. J.; Van Gerven, B. C. B.; Estirado, E. M.; Milroy, L.-G.; Merkx, M. Semisynthetic Bioluminescent Sensor Proteins for Direct Detection of Antibodies and Small Molecules in Solution. *ACS Sensors* **2017**, *2*, 1730−1736.
(22) Li, Y.; Gabriele, E.; Samain, F.; Favalli, N.; Sladojevich, F.; Scheuermann, J.; Neri, D. Optimized Reaction Conditions for Amide Bond Formation in DNA-Encoded Combinatorial Libraries. *ACS Comb. Sci.* **2016**, *18*, 438−443.
(23) Damodaran, V. B.; Murthy, S. N. Bio-Inspired Strategies for Designing Antifouling Biomaterials. *Biomater. Res.* **2016**, *20*, 18.
(24) Camós Noguer, A.; Olsen, S. M.; Hvilsted, S.; Kiil, S. Long-Term Stability of PEG-Based Antifouling Surfaces in Seawater. *J. Coatings Technol. Res.* **2016**, *13*, 567−575.
(25) Kulkarni, T.; Slaughter, G. Application of Semipermeable Membranes in Glucose Biosensing. *Membranes* **2016**, *6*, 55.
(26) Klaus, S.; Heringlake, M.; Bahlmann, L. Bench-to-Bedside Review: Microdialysis in Intensive Care Medicine. *Critical Care* **2004**, *8*, 363−368.
(27) Lundberg, G.; Wahlberg, E.; Swedenborg, J.; Sundberg, C. J.; Ungerstedt, U.; Olofsson, P. Continuous Assessment of Local Metabolism by Microdialysis in Critical Limb Ischaemia. *Eur. J. Vasc. Endovasc. Surg.* **2000**, *19*, 605−613.
(28) Kilic, T.; Navaee, F.; Stradolini, F.; Renaud, P.; Carrara, S. Organs-on-Chip Monitoring: Sensors and Other Strategies. *Microphysiological Syst.* **2018**, *1*, 1.
(29) Zhao, Y.; Kankala, R.; Wang, S.-B.; Chen, A.-Z. Multi-Organs-on-Chips: Towards Long-Term Biomedical Investigations. *Molecules* **2019**, *24*, 675.
(30) Li, X.; Soler, M.; Szydzik, C.; Khoshmanesh, K.; Schmidt, J.; Yesilkoy, F.; Belushkin, A.; Coukos, G.; Mitchell, A.; Altug, H. *An Integrated Nanoplasmonic Biosensor for Monitoring Cytokine Secretion from Single Cells*; Institute of Electrical and Electronics Engineers (IEEE), 2019; pp 113−116.
(31) McKeating, K. S.; Aubé, A.; Masson, J.-F. Biosensors and Nanobiosensors for Therapeutic Drug and Response Monitoring. *Analyst* **2016**, *141*, 429−449.
(32) Simon, L. L.; Pataki, H.; Marosi, G.; Meemken, F.; Hungerbühler, K.; Baiker, A.; Tummala, S.; Glennon, B.; Kuentz, M.; Steele, G.; et al. Assessment of Recent Process Analytical Technology (PAT) Trends: A Multiauthor Review. *Organic Process Research Development* **2015**, *19*, 3−62.

https://dx.doi.org/10.1021/acssensors.0c00220
ACS Sens. 2020, 5, 1168−1176